Tonsil-derived mesenchymal stem cell-derived extracellular vesicles suppress MAPK-NF-κB signaling and restore osteogenic differentiation in LPS-stimulated periodontal ligament fibroblasts

WON-JUNG BAE[1*], SU KANG KIM[2*], HAN-SOO KIM[3], SANG WOOK KANG[4] and JU YEON BAN[1]

[1]Department of Dental Pharmacology, College of Dentistry, Dankook University, Cheonan, Chungcheongnam-do 31116, Republic of Korea;
[2]Department of Biomedical Laboratory Science, Catholic Kwandong University, Gangneung, Gangwon-do 25601, Republic of Korea;
[3]Department of Biomedical Sciences, Catholic Kwandong University, Gangneung, Gangwon-do 25601, Republic of Korea;
[4]Department of Oral and Maxillofacial Pathology, College of Dentistry, Kyung Hee University, Seoul 02447, Republic of Korea

Received November 26, 2025; Accepted February 4, 2026

DOI: 10.3892/mmr.2026.13860

Abstract. The present study evaluated and compared the anti-inflammatory and osteogenic effects of extracellular vesicles (EVs) derived from tonsil-derived mesenchymal stem cells (T-MSC-EVs) in a lipopolysaccharide (LPS)-induced *in vitro* model of periodontitis using human periodontal ligament fibroblasts (hPDLFs). hPDLFs were treated with LPS to induce inflammation, followed by treatment with T-MSC-EVs. Cell viability was assessed using a 3-(4,5-dimethylthiazol-2-yl)-2,5-diphenyltetrazolium bromide assay. The expression levels of inflammatory cytokines (*IL-1β*, *IL-6*, *IL-8* and *IFN-γ*) and osteogenic markers [alkaline phosphatase (*ALP*), bone sialoprotein, osteopontin, osteocalcin and sclerostin] were evaluated using reverse transcription-quantitative PCR. Inflammatory signaling proteins (phosphorylated ERK, phosphorylated JNK, c-Fos, c-Jun and NF-κB) were analyzed by western blotting. Osteogenic activity was assessed using an ALP activity assay and alizarin red staining over 21 days. Treatment with T-MSC-EVs significantly protected hPDLFs from LPS-induced growth suppression. T-MSC-EVs exhibited selective immunomodulation, reducing IL-8 and IFN-γ expression, while preserving IL-6 and IL-1β expression, which was accompanied by inhibited MAPK-activator protein 1 and NF-κB signaling. Finally, T-MSC-EVs restored the osteogenic potential by recovering ALP activity, mineral deposition and expression of osteogenic marker genes repressed by LPS. These findings underscore the therapeutic potential of EVs as next-generation biologics for periodontitis and emphasize the importance of selecting appropriate EV sources to achieve targeted immune modulation and tissue regeneration.

Correspondence to: Professor Sang Wook Kang, Department of Oral and Maxillofacial Pathology, College of Dentistry, Kyung Hee University, 26 Kyungheedae-ro, Dongdaemun-gu, Seoul 02447, Republic of Korea
E-mail: pathemis@khu.ac.kr

Professor Ju Yeon Ban, Department of Dental Pharmacology, College of Dentistry, Dankook University, 119 Dandae-ro, Dongnam-gu, Cheonan, Chungcheongnam-do 31116, Republic of Korea
E-mail: jyban@dankook.ac.kr

*Contributed equally

Key words: extracellular vesicles, periodontitis, inflammation, stem cells, osteogenesis

Introduction

Periodontitis is one of the most common chronic inflammatory diseases worldwide and a leading cause of tooth loss in adults (1). Its prevalence is steadily increasing among aging populations, with significant effects not only on oral health but also on overall health and quality of life. Periodontitis is also associated with systemic chronic inflammatory diseases, including inflammatory bowel disease (IBD), cardiovascular disease, autoimmune conditions, and Alzheimer's disease (2). Furthermore, the increasing incidence of periodontitis has led to an increase in healthcare costs (3). Periodontitis is caused by oral bacteria, whereby complex interactions between the host immune response and bacterial toxins lead to chronic inflammation (4). This results in alveolar bone destruction and the loss of tooth-supporting tissues, ultimately leading to tooth loss (5). Therefore, early periodontitis prevention and delaying progression are crucial for maintaining oral health and improving patient quality of life in later life.

The periodontal ligament (PDL) plays a key role in periodontitis pathophysiology. The PDL is a connective tissue attaching teeth to the alveolar bone. In addition to its roles in alleviating mechanical stress and transmitting sensations, the PDL also helps regulate immune responses and inflammation. In particular, in early-stage periodontitis, bacterial stimulation activates PDL cells to secrete various inflammatory cytokines [interleukin (IL)-1β, IL-6, tumor necrosis factor (TNF)-α, etc.] and matrix-degrading enzymes (MMPs) to induce an inflammatory response and promote alveolar bone destruction (6,7).

Therefore, inflammation-inducing models using PDL cells are important experimental tools in periodontitis research. Among these models, lipopolysaccharide (LPS) is a toxin derived from the cell wall of gram-negative bacteria, such as *Porphyromonas gingivalis*, and is a major causative agent of periodontitis. It induces a strong inflammatory response by activating inflammatory signaling pathways [mitogen-activated protein kinase (MAPK) and nuclear factor-κB (NF-κB), etc.] through the innate immune receptor Toll-like receptor 4 (TLR4) (8). Therefore, LPS is the most widely used stimulant in *in vitro* inflammatory models mimicking periodontitis, producing an inflammatory response similar to that of periodontitis (9).

Recent studies have increasingly focused on the regulatory effects of extracellular vehicles (EVs) on inflammatory diseases. EVs, including small vesicles often referred to as exosomes (30-150 nm), are secreted by various cell types and carry bioactive molecules such as mRNA, miRNA, and proteins, thereby mediating intercellular communication and regulating target cell function (10). Stem cell-derived EVs have been shown to exert anti-inflammatory and tissue regeneration-promoting effects in several disease models (11). Among these, EVs derived from tonsil-derived stem cells (T-MSC-EVs) modulate immune cell function, suppress pro-inflammatory cytokine production, and promote tissue repair (12,13).

Given that periodontitis is characterized by both excessive inflammation and impaired tissue regeneration, therapeutic strategies that simultaneously suppress inflammation and support osteogenic repair are of particular interest. Therefore, this study investigated the dual anti-inflammatory and osteogenic effects of T-MSC-EVs in an LPS-stimulated human periodontal ligament fibroblast (hPDLF) model of periodontitis.

Materials and methods

Cell culture. The hPDLFs were commercially obtained as primary cells from company (hPDLF, #2630, ScienCell Research Laboratories). This cell type was classified as a primary human cell tissue and was not immortalized cell lines. Detailed product information is available at the supplier's website: https://sciencellonline.com/en/human-periodontal-ligament-fibroblasts/. Although the cells were commercially sourced, the study was conducted in accordance with the Declaration of Helsinki and the research design was officially approved by the Institutional Review Board of Kyung Hee University (IRB No. KHSIRB-25-417). The hPDLF cells were cultured in Dulbecco's Modified Eagle's Medium (DMEM) supplemented with 10% fetal bovine serum (FBS), 100 U/ml penicillin, and 100 μg/ml streptomycin in a humidified atmosphere of 5% CO_2 at 37˚C. Osteogenic medium (OM) was prepared by supplementing culture media with 50 μg/ml L-ascorbic acid (Sigma-Aldrich; Merck KGaA) and 10 mM β-glycerophosphate (Sigma-Aldrich; Merck KGaA) (14). The hPDLF cells were sub-cultured at 80-90% confluence, and experiments were conducted using passages 4-7.

EV preparation from T-MSCs and characterization by nanoparticle tracking analysis (NTA) and transmission electron microscopy (TEM). T-MSCs were obtained from human tonsil tissues, following approval by the Institutional Review Board (Department of Otorhinolaryngology, Yonsei University Wonju College of Medicine, IRB-CR320104), with written informed consent obtained from all donors. This cell type was classified as a primary human cell tissue and was not immortalized cell lines. T-MSCs were cultured in medium supplemented with EV-depleted FBS prepared by ultracentrifugation, as previously described. At 70-80% confluency, the cells were washed, switched to fresh EV-depleted medium, and conditioned for 24-48 h. Conditioned medium (CM) was collected and cleared of cells, apoptotic bodies, and debris by sequential low- to medium-speed centrifugation and 0.22 μm filtration. Small EVs were then isolated from the clarified CM by high-speed ultracentrifugation, washed by a second ultracentrifugation step, and resuspended in Dulbecco's PBS (DPBS). The resulting EVs were then aliquoted and stored at -80˚C while minimizing freeze-thaw cycles. The T-MSC-EVs used in the experiments in the present study were manufactured and purified by Hyundai Meditech Co., Ltd. using internal standard operating procedures (SOPs). EV identity, particle size distribution, and concentration were confirmed by nanoparticle tracking analysis (NTA). Transmission electron microscopy (TEM) was performed using a Talos L120C microscope (FEI, USA) operated at 120 kV with a LaB_6 electron gun. A carbon-film-coated copper grid (400 mesh, Ted Pella) was rendered hydrophilic using a PELCO easiGlow™ glow discharge system (Ted Pella) under negative polarity for 20 sec before mounting the samples. For negative staining, a 2% uranyl acetate (UA) solution was freshly prepared. One drop of EV suspension was placed on a glow-discharged grid and incubated for approximately 1 min. Excess liquid was gently removed using filter paper. The grid was then floated on a 20 μl droplet of 2% UA solution for 20 sec for staining, and excess stain was blotted off. Finally, the grid was air-dried for 10 min at room temperature before imaging.

EV dosing. T-MSC-EVs were quantified by NTA and administered to hPDLFs at final concentrations of $1x10^8$ or $5x10^8$ particles/ml, depending on the experimental condition. Particle number-based dosing was used because the total EV protein content was insufficient for reliable quantification and did not necessarily reflect the number of vesicles or functional EV cargo. The selection of these specific doses ($1x10^8$ or $5x10^8$ particles/ml) was based on previous studies demonstrating that MSC-derived EVs exert significant immunomodulatory effects within this concentration range in in-vitro human cell models (15).

RT-qPCR. Total RNA was isolated from cells using TRIzol reagent (Invitrogen, Carlsbad, CA, USA) according to the manufacturer's instructions. Reverse transcription was performed using AccuPower RT PreMix (Bioneer). qPCR was performed on the cDNA samples using Axen™ qPCR Master Mix (Macrogen) on a 7500 Real-Time PCR System (Thermo Fisher Scientific, Inc.). The relative mRNA levels of target genes were normalized to β-actin mRNA levels and analyzed using the comparative Ct method (ΔΔCt) (16). The primer sequences used in this study are listed in Table I.

Table I. PCR primers.

Gene	Sequences (5'-3')	Ta, ˚C	Size, bp
GAPDH	Forward: CTCTTCACCACCATGGAGAAG	60	201
	Reverse: GTTGTCATGGATGACCTTGGC		
IFN-γ	Forward: TGTCGCCAGCAGCTAAAACA	60	91
	Reverse: TGCAGGCAGGACAACCATTA		
IL-6	Forward: CACCGGGAACGAAAGAGAAGC	61	75
	Reverse: CGAAGGCGCTTGTGGAGA		
IL-1β	Forward: AGCTACGAATCTCCGACCAC	59	186
	Reverse: CGTTATCCCATGTGTCGAAGAA		
ALP	Forward: CTATCCTGGCTCCGTGCTCC	62	133
	Reverse: AGAGATGCAATCGACGTGGG		
BSP	Forward: GACACCACAGAGACCGGAAG	60	232
	Reverse: AATTGTCCCCACGAGGTTCC		
OCN	Forward: ATGAGAGCCCTCACACTCCT	59	117
	Reverse: CTTGGACACAAAGGCTGCAC		
OPN	Forward: ACAAATACCCAGATGCTGTGGC	61	86
	Reverse: ACTTGGAAGGGTCTGTGGGG		
SOST	Forward: ACACAGCCTTCCCGTGTAGTG	62	187
	Reverse: CGGACACGTCTTTGGTCTCA		

ALP, alkaline phosphatase; BSP, bone sialoprotein; OCN, osteocalcin; OPN, osteopontin; SOST, sclerostin; Ta, annealing temperature.

Western blotting. Total cells were lysed in radioimmunoprecipitation assay (RIPA) buffer supplemented with protease and phosphatase inhibitor cocktails. Whole-cell lysates and nuclear extracts were prepared according to standard protocols. Protein concentrations were determined using a protein assay. Equal amounts of protein (25 μg per lane) were separated by sodium dodecyl sulfate-polyacrylamide gel electrophoresis (SDS-PAGE) and transferred onto polyvinylidene fluoride (PVDF) membranes. After transfer, the membranes were rinsed three times with Tris-buffered saline containing 0.1% Tween-20 (TBST) and blocked with a blocking solution for 1 h at room temperature. The membranes were then incubated overnight at 4˚C with primary antibodies, followed by incubation with horseradish peroxidase-conjugated secondary antibodies for 1 h at 37˚C. Primary antibodies against β-actin, p65, c-Jun, and c-Fos (Santa Cruz Biotechnology, Inc.), as well as phosphorylated or total extracellular signal-regulated kinase (ERK) and c-Jun N-terminal kinase (JNK) (Cell Signaling Technology) were used at a dilution of 1:1,000.

For characterization, EVs were lysed in RIPA buffer containing protease inhibitors, and protein concentrations were determined. Equal amounts of vesicle proteins were subjected to SDS-PAGE and transferred onto PVDF membranes, as described above. The membranes were probed with primary antibodies against the exosome markers cluster of differentiation (CD)63 (rabbit monoclonal, Cell Signaling Technology, #52090, 1:1,000) and CD9 (rabbit monoclonal, #13174, 1:1,000). Albumin (rabbit polyclonal, #4929; Cell Signaling Technology, 4929, 1:1,000) was used as a negative marker to evaluate contamination by soluble serum proteins. Protein bands were visualized using an enhanced chemiluminescence (ECL) detection system (Amersham), and images were captured using an Amersham™ ImageQuant™ 500 imaging system (Cytiva).

Cell proliferation. Cell proliferation was evaluated using EZ-Cytox (DoGenBio), according to the manufacturer's instructions. Briefly, cells were seeded in 96-well plates at a density of $5x10^3$ cells/well and cultured under the indicated conditions. At the designated time points, 100 μl of solution, diluted 1:10, was added to the culture was added to each well and incubated for 1 h at 37˚C. The absorbance at 450 nm was measured using a microplate reader (Thermo Fisher Scientific, Inc.). Cell proliferation was expressed as a percentage relative to the control group. All experiments were performed in triplicate.

Alkaline phosphatase (ALP) activity assay and staining. ALP activity was measured using a sensoLyte® pNpp alkaline phosphatase assay kit (Anaspec). Cells were cultured in 96-well plates, and osteogenic differentiation was induced under the specified conditions. After the designated incubation period, the culture medium was removed, and the cells were gently washed twice with PBS to eliminate serum components that could interfere with the assay. Subsequently, 100 μl of pNPP substrate solution was directly added to each well. The plate was then incubated at room temperature for 1 h, protected from light, and quantified by measuring absorbance at 405 nm using a microplate reader. ALP staining was performed using a TRACP & ALP double staining kit (Takara) according to the manufacturer's instructions. The cells were fixed in a fixation solution for 20 min, washed twice with PBS, and stained with ALP staining solution. After incubation in the dark at room

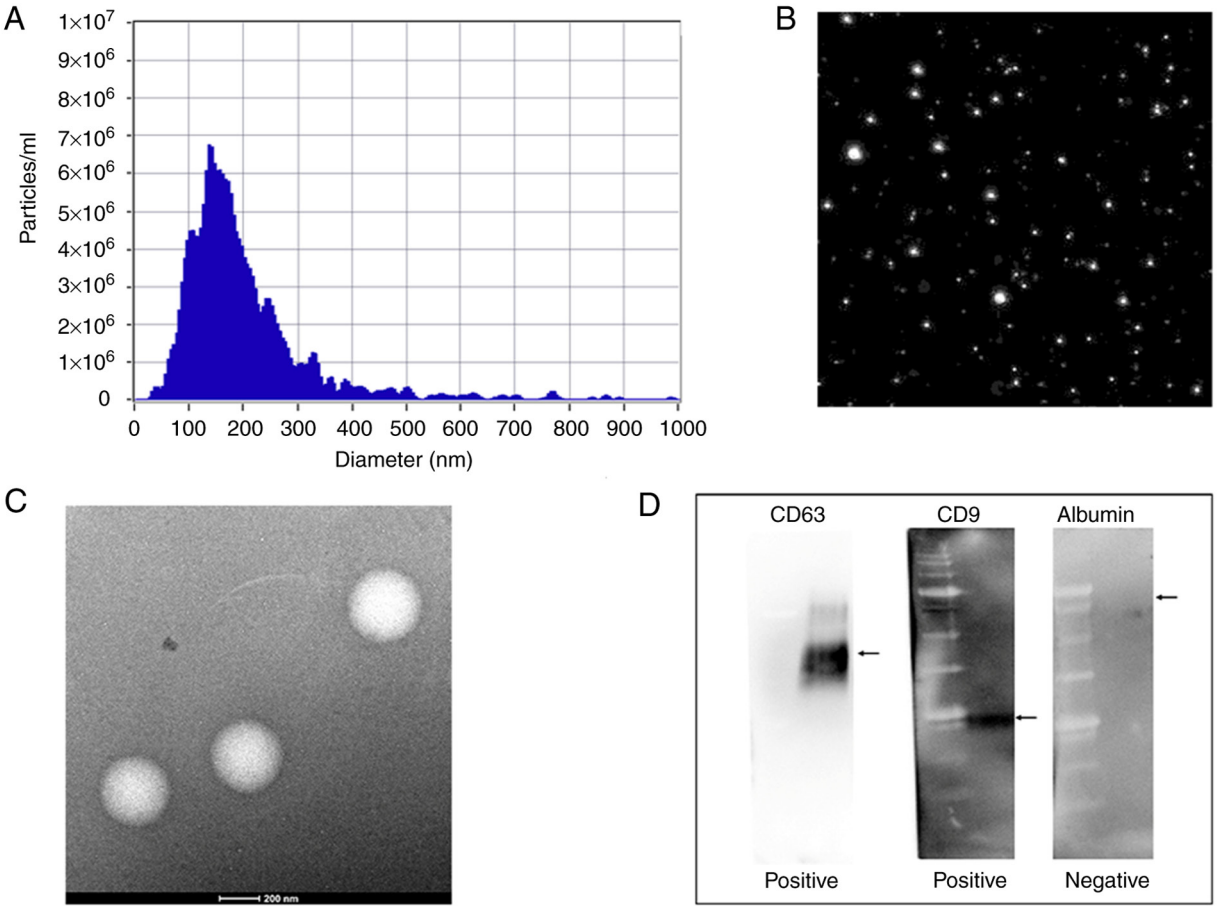

Figure 1. Data demonstrating the successful isolation of T-MSC-derived EVs exhibiting typical exosomal size, morphology and markers. (A) NTA showing the particle size distribution of EVs isolated from T-MSCs. The diameter of the majority of particles ranged between 50 and 150 nm. (B) Representative NTA image showing isolated T-MSC-derived EVs obtained using a ZetaView instrument (Particle Metrix GmbH) equipped with a 488 nm laser. (C) Transmission electron microscopy image showing the presence of round, vesicle-like structures with sizes consistent with exosomes. Scale bar, 200 nm. (D) Western blot analysis of EV-associated markers demonstrating the presence of the exosomal markers CD63 and CD9 and the absence of albumin, a negative marker for soluble protein contamination, confirming the purity of the isolated EVs. EV, extracellular vesicle; NTA, nanoparticle tracking analysis; T-MSC, tonsil-derived mesenchymal stem cell.

temperature for 1 h, the stained cells were photographed under a light microscope (ECLIPSE TS100; Nikon).

Alizarin Red staining. Calcium deposition was assessed by Alizarin Red S staining. Cells were cultured in 24-well plates, and osteogenic differentiation was induced under the specified conditions. The cells were then washed twice with PBS and fixed in 70% ethanol for 20 min at room temperature. After fixation, the cells were rinsed with distilled water and incubated with Alizarin Red S solution (Samchun Pure Chemical) for 2 h in the dark at room temperature. The stained cells were washed thoroughly with distilled water to remove excess dye and then air-dried. The stained calcium deposits were imaged using an ECLIPSE TS100 system (Nikon).

Statistical analysis. Statistical analyses were performed using GraphPad Prism, version 8.4.3 (GraphPad Software). For the mRNA expression of inflammatory markers (PCR data), ordinary one-way analysis of variance (ANOVA) was performed, followed by Bonferroni's post-hoc test. For all other experiments, two-way ANOVA with Tukey's multiple comparison test was used. All values of $^{*}P<0.05$, $^{**}P<0.01$, $^{***}P<0.001$, $^{****}P<0.0001$ were regarded as indicative of statistical significance.

Results

NTA characterization of marker validation and T-MSC-derived EVs. NTA, TEM, and western blotting were performed to confirm the physical characteristics and molecular identity of T-MSC-derived EVs (Fig. 1). The NTA analysis considered only particles ≤200 nm as EV-sized populations; additionally, minor high-diameter shoulders (>250 nm) were excluded as potential aggregates. The size-concentration curve showed a unimodal distribution with a peak at approximately 140-150 nm. The particle concentration was approximately $1.5x10^8$ particles/ml. Consistent with these measurements, TEM revealed round vesicle-like structures within the expected exosomal size range (50-150 nm). The isolated T-MSC-derived EVs showed a typical exosomal morphology without apparent aggregation. Western blotting to assess the expression of EV-associated markers and to further validate the exosomal nature and purity of the isolated vesicles revealed tetraspanins CD63 and CD9 in the T-MSC-derived EVs, confirming the enrichment of exosome-associated proteins. In contrast, albumin, which was used as a negative marker for soluble protein contamination, was not detected in the EV preparations.

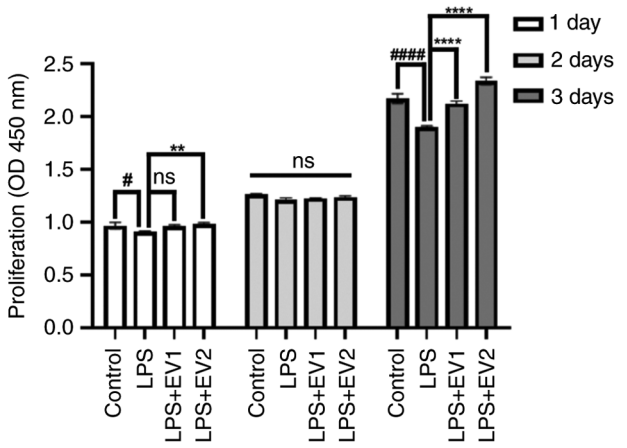

Figure 2. Cell proliferation was evaluated by measuring the OD at 450 nm on days 1, 2 and 3 following treatment with LPS (1 μg/ml) and T-MSC-EVs. EVs were used at concentrations of $1x10^8$ particles/ml or $5x10^8$ particles/ml. LPS treatment suppressed proliferation in a time-dependent manner, with a pronounced reduction observed on day 3 (P<0.0001 vs. control). By contrast, EV treatment effectively prevented LPS-induced proliferation inhibition, and notably, treatment with T-MSC-EVs at $5x10^8$ particles/ml resulted in a significant increase in cell proliferation beyond the control level on day 3. No significant differences were observed among the groups on day 2. All experiments were performed in triplicate. $^{\#}$P<0.05 and $^{\#\#\#\#}$P<0.0001, control group vs. LPS group. **P<0.01 and ****P<0.0001, LPS group vs. EV-treated groups. EV1, T-MSC-derived EVs ($1x10^8$ particles/ml); EV2, T-MSC-derived EVs ($5x10^8$ particles/ml); EV, extracellular vesicle; LPS, lipopolysaccharide; ns, not significant; OD, optical density; T-MSC, tonsil-derived mesenchymal stem cell.

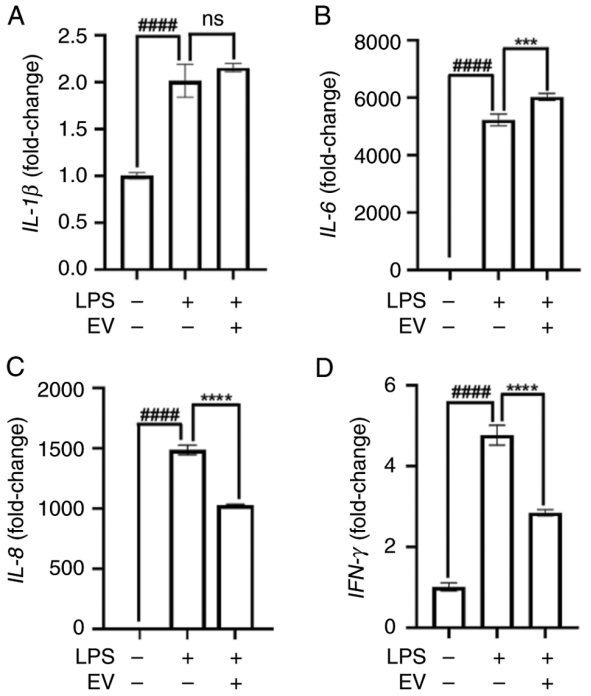

Figure 3. Quantitative PCR analysis of proinflammatory cytokines (*IL-1β, IL-6, IL-8* and *IFN-γ*) in cells stimulated with LPS (1 μg/ml), with or without tonsil-derived mesenchymal stem cell-derived EVs ($5x10^8$ particles/ml) treatment. (A) *IL-1β* mRNA expression. (B) *IL-6* mRNA expression. (C) *IL-8* mRNA expression. (D) *IFN-γ* mRNA expression. LPS significantly induced the expression of all four cytokines. EV treatment further increased *IL-6* expression but had no significant effect on *IL-1β*. By contrast, *IL-8* and *IFN-γ* levels were significantly decreased following EV treatment, suggesting partial attenuation of the inflammatory response. All experiments were performed in triplicate. $^{\#\#\#\#}$P<0.0001, control group vs. LPS group. ***P<0.001 and ****P<0.0001, LPS group vs. EV-treated group. EV, extracellular vesicle; LPS, lipopolysaccharide; ns, not significant.

Collectively, these results demonstrated that the isolated T-MSC-derived EVs exhibited the size distribution, morphology, and molecular marker profile characteristic of exosomes, indicating successful isolation and high purity (Fig. 1).

LPS inhibition of cell proliferation and the protective effect of EVs. Fig. 2 shows the effects of LPS and EVs on the PDL. LPS inhibited cell proliferation in a time- and dose-dependent manner. Although no significant differences were observed on day 2, marked differences were observed among the groups on day 3. T-MSC-EVs effectively prevented the LPS-induced inhibition of cell proliferation at both concentrations, and higher concentrations promoted cell growth to a level exceeding that of the control.

Changes in inflammatory cytokine expression. The expression levels of inflammatory cytokines, including *IL-1β, IL-6, IL-8*, and *IFN-γ*, were markedly elevated following LPS stimulation in hPDLFs (Fig. 3). In the T-MSC-EVs-treated group, *IL-6* and *IL-1β* levels were stable or slightly increased, with no statistically significant change in *IL-1β*, while T-MSC-EV treatment significantly reduced *IL-8* and *IFN-γ* levels. These results demonstrated a cytokine response pattern characterized by selective reduction of *IL-8* and *IFN-γ* in the experiment.

Modulation of inflammatory signaling pathways. LPS stimulation activated classical MAPK pathways, including JNK and ERK, which mediate inflammatory responses and lead to the activation of transcription factors, including AP-1 (c-Jun, c-Fos) and NF-κB (Fig. 4). The EV-treated group showed markedly decreased phosphorylation of MAPK components (ERK and JNK), suggesting that T-MSC-EVs suppressed the upstream inflammatory signaling cascade (Fig. 4A). Furthermore, downstream transcription factors c-Jun, c-Fos, and NF-κB were also inhibited, supporting the anti-inflammatory effects of T-MSC-EVs (Fig. 4B).

Restoration of osteogenic activity by EV treatment under inflammatory conditions. The effects of T-MSC-EVs on bone formation were evaluated using ALP activity assay, ALP staining, and Alizarin Red staining over 21 days. LPS treatment markedly reduced ALP activity and mineralization capacity (Fig. 5). However, T-MSC-EV treatment restored or even enhanced ALP activity and mineralized nodule formation, especially at later time points (days 14 and 21), indicating a potential osteogenic effect of T-MSC-EVs despite inflammatory conditions.

EVs restore osteogenic gene expression suppressed by LPS treatment. Fig. 6 shows changes in gene expression induced by LPS and T-MSC-EVs. LPS treatment resulted in an overall decrease in the mRNA expression of key osteogenic genes, including *ALP*, *BSP*, *OPN*, and *OCN*, with *BSP* and *OPN* exhibiting a more pronounced suppression trend over time. In contrast, treatment with EVs resulted in recovered or increased gene expression, with a significant level of recovery observed

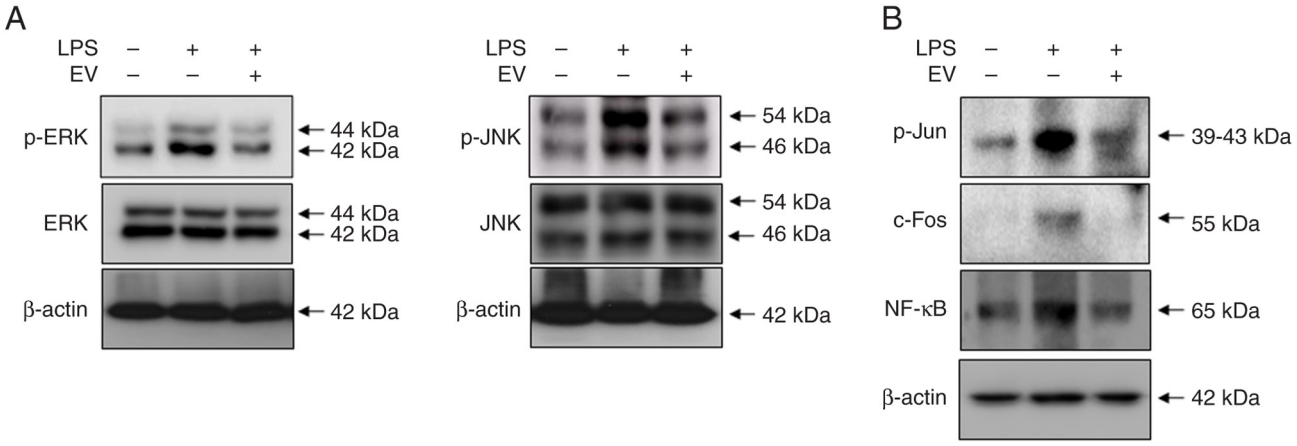

Figure 4. Western blot analysis showing phosphorylation levels of MAPK pathway proteins (p-ERK and p-JNK), as well as downstream transcription factors (c-Jun, c-Fos and NF-κB) following LPS (1 μg/ml) stimulation, with or without tonsil-derived mesenchymal stem cell-derived EVs ($5x10^8$ particles/ml) treatment. (A) p-ERK and p-JNK protein levels. (B) c-Jun, c-Fos and NF-κB protein expression. LPS treatment markedly increased the phosphorylation of MAPK proteins and the expression of transcription factors, whereas EV treatment suppressed these changes. β-actin was used as a loading control. To ensure accuracy, target proteins and their respective loading controls (β-actin) were derived from the same experimental run and processed under identical conditions. All experiments were performed in triplicate. EV, extracellular vesicle; LPS, lipopolysaccharide; p-, phosphorylated.

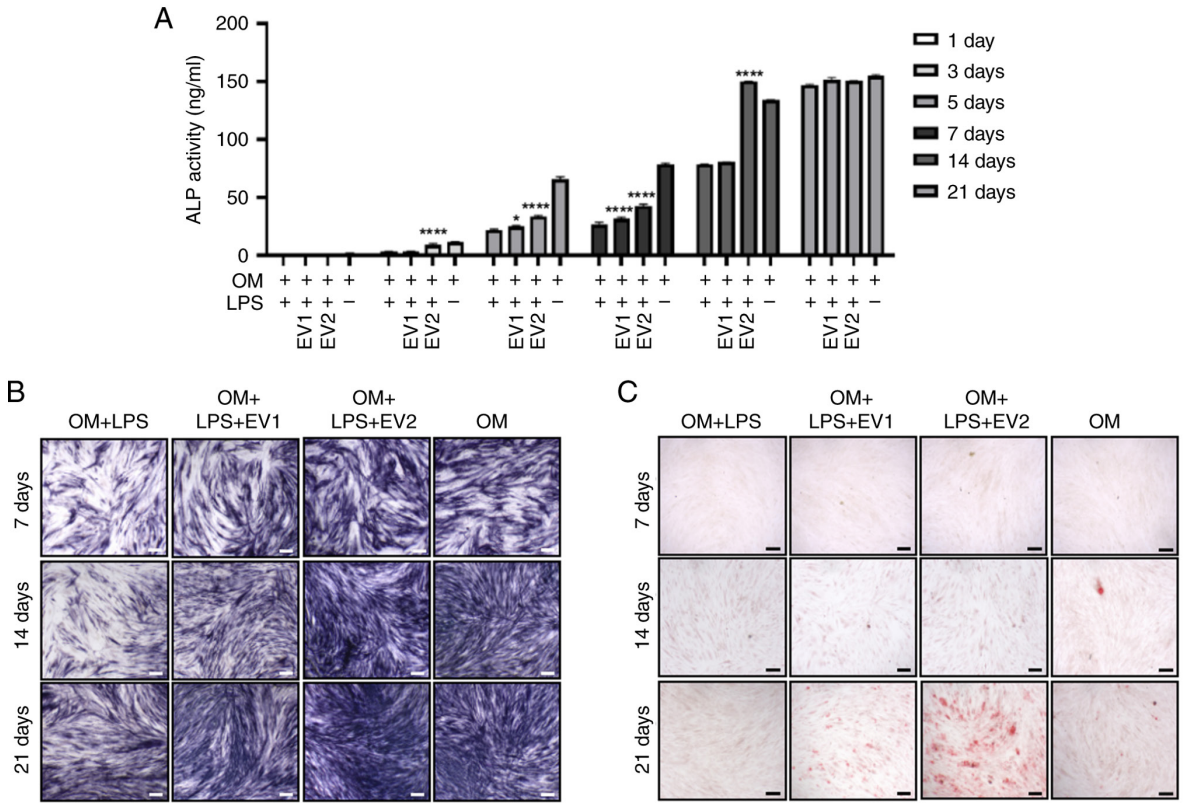

Figure 5. T-MSC-derived EVs restore osteogenic activity under LPS stimulation. (A) An ALP activity assay was performed at 1, 3, 5, 7, 14 and 21 days. ALP activity remained suppressed in the LPS (1 μg/ml)-treated group compared with the OM group up to day 14. By contrast, compared with the LPS-treated group, in the EV1-treated group, ALP activity was significantly increased at day 5. In the EV2-treated group, LPS-suppressed ALP activity was significantly restored at day 3. (B) The ALP staining intensity was reduced in the LPS group, which was reversed by EV treatment. Scale bar, 200 μm. (C) Alizarin red staining revealed decreased mineralization in the LPS group at 21 days, while EV treatment restored calcium deposition, suggesting enhanced bone formation capacity. Scale bar, 200 μm. All experiments were performed in triplicate. *P<0.05, ****P<0.0001, OM + LPS group vs. OM + LPS + EV-treated groups. ALP, alkaline phosphatase; EV1, T-MSC-derived EVs ($1x10^8$ particles/ml); EV2, T-MSC-derived EVs ($5x10^8$ particles/ml); EV, extracellular vesicle; LPS, lipopolysaccharide; OM, osteogenic medium; T-MSC, tonsil-derived mesenchymal stem cell.

for some indicators. In particular, *OPN* and *OCN*, which are mid- and late-stage osteogenic differentiation markers (17,18), showed a tendency for expression to increase rapidly after 14 days due to T-MSC-EVs. The levels of *SOST*, an osteogenic inhibitor (19), increased following LPS treatment but were suppressed again upon T-MSC-EV treatment, suggesting the positive effect of EVs on the normal regulation of osteogenic gene expression, even under inflammatory conditions.

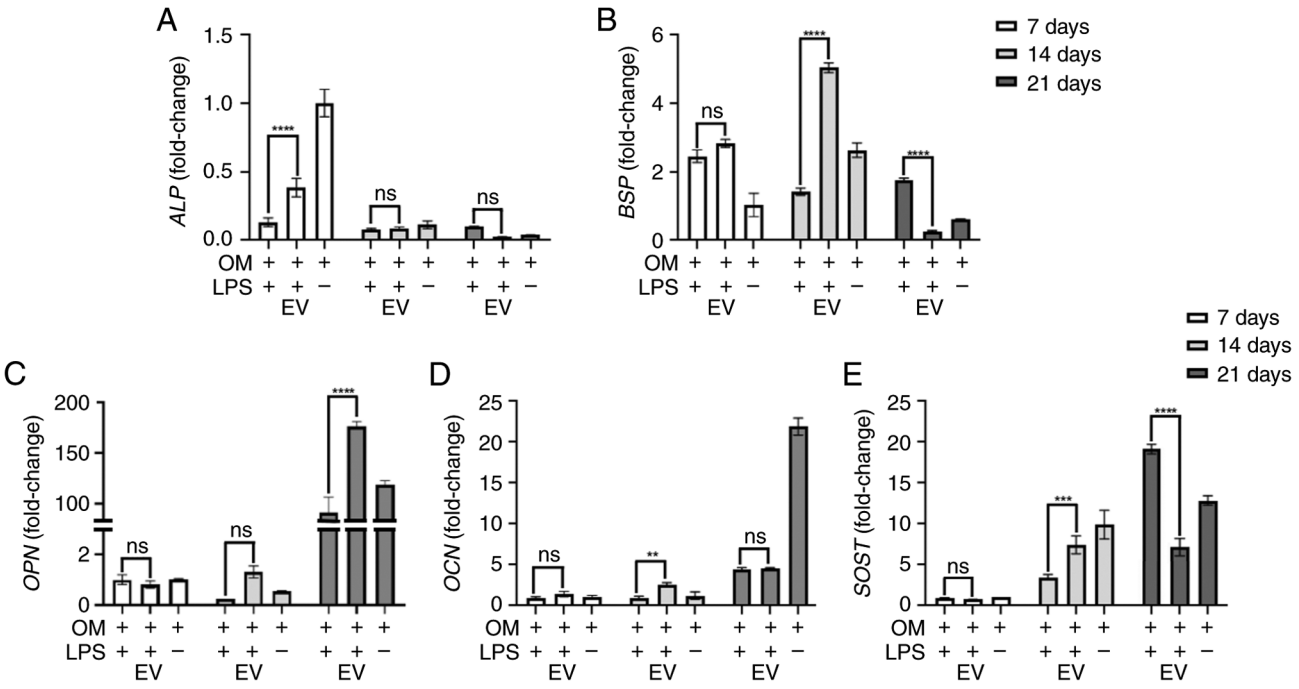

Figure 6. Reverse transcription-quantitative PCR analysis of osteogenic markers was conducted at 7, 14 and 21 days after treatment. (A) *ALP* mRNA expression. (B) *BSP* mRNA expression. (C) *OPN* mRNA expression. (D) *OCN* mRNA expression. (E) *SOST* mRNA expression. *ALP* gene expression, which was reduced by LPS (1 μg/ml) treatment, was enhanced by tonsil-derived mesenchymal stem cell-derived EVs (5x10^8 particles/ml) at day 7. *BSP* and *OCN* gene expression was increased following LPS + EV treatment at day 14; however, *BSP* expression was lower in the EV-treated group than in the LPS-treated group at day 21. *SOST* expression was markedly higher in the EV-treated group than in the LPS-treated group at day 14, whereas at day 21, *SOST* expression was significantly higher in the LPS-treated group. All experiments were performed in triplicate. **P<0.01, ***P<0.001, ****P<0.0001, OM + LPS group vs. OM + LPS + EV-treated group. *ALP*, alkaline phosphatase; *BSP*, bone sialoprotein; EV, extracellular vesicle; LPS, lipopolysaccharide; ns, not significant; *OCN*, osteocalcin; OM, osteogenic medium; *OPN*, osteopontin; *SOST*, sclerostin.

Discussion

In present study, we evaluated the regulatory effects and underlying mechanisms of EVs derived from T-MSC on LPS-induced inflammation in hPDLFs. T-MSCs represent an attractive source of stem cell because they can be obtained as surgical waste after tonsillectomy, providing an easily accessible and ethically favorable material. Additionally, T-MSCs are characterized by a strong proliferative capacity and an immune-privileged phenotype, which endows their EVs with enhanced immunomodulatory and regenerative potential.

LPS activates innate immunity through TLR4, leading to NF-κB and MAPK (p38, ERK, and JNK) signaling, which promotes inflammatory cytokine production, inhibits cell proliferation, and induces cell damage (20). Our findings showed that T-MSC-EVs restored the LPS-induced suppression of hPDLF proliferation. This protective effect was more evident at higher particle doses.

T-MSC-EVs selectively modulated inflammatory cytokines by suppressing *IL-8* and *IFN-γ*, key mediators of neutrophil recruitment and Th1 signaling (21,22), while generally maintaining *IL-6* and *IL-1β* levels, which are essential for immune activation and tissue repair (23). This selective cytokine regulation, combined with EV-mediated inhibition of MAPK-AP-1 components (p-ERK, p-JNK, c-Fos, c-Jun), suggests that EVs attenuate excessive inflammation while preserving pro-repair signals (24).

In addition to controlling inflammation, T-MSC-EVs also restored osteogenic activity under inflammatory conditions. ALP activity and mineralized nodule formation were significantly enhanced at later stages, and key osteogenic genes (*ALP, BSP, OPN,* and *OCN*) showed marked recovery. Particularly, *OPN* and *OCN*, which are markers of mid-to-late osteogenic differentiation, were robustly reactivated (17,18). Moreover, *SOST*, a negative regulator of bone formation, was suppressed following T-MSC-EV treatment (19). These findings indicate that T-MSC-EVs not only protect cells from inflammatory insults but also actively promote bone regeneration by reinstating osteogenic gene expression profiles.

Although the present study did not analyze the EV cargo, the same T-MSC-EVs were previously reported to contain multiple highly expressed miRNAs (25) including miR-199a-3p, miR-145-5p, miR-24-3p, miR-214-3p, and let-7 family members. These enriched miRNAs may target components of the MAPK-AP-1 and TLR4-associated NF-κB pathways in hPDLFs, contributing to the selective reduction of IL-8 and IFN-γ and to the reversal of LPS-induced proliferation and osteogenic suppression. However, whether the miRNA and protein cargo profiles of T-MSC-EVs in the present study, and their functional relevance, are fully consistent with those reported previously remains to be directly validated.

Several studies have reported the anti-inflammatory and regenerative effects of EVs derived from various stem cell sources (26-29). In the present study, T-MSC-EVs exhibited significant immunomodulatory and regenerative potential, likely attributable to the immune-privileged

nature of tonsil-derived cells and the enriched expression of immune-regulatory genes (30,31). These findings highlight the importance of selecting an appropriate source of EVs. Nevertheless, challenges remain, including heterogeneous EV composition, inconsistent therapeutic efficacy, lack of standardized quantification protocols, and limitations in large-scale production and storage stability (32). Addressing these issues is critical for a successful clinical translation.

In summary, EVs derived from T-MSCs restored cell viability, attenuated tissue-destructive cytokines, and preserved regeneration-associated immune responses. They also inhibited the MAPK-AP-1 signaling pathway and promoted osteogenic differentiation, even under inflammatory conditions. These multifaceted actions highlight T-MSC-EVs as intelligent biological modulators that can fine-tune the immune response while also supporting tissue regeneration. Higher concentrations of T-MSC-EVs enhanced cell proliferation and differentiation. Future studies should aim to elucidate active cargo components (e.g., miRNAs and proteins), standardize production and quality control processes, and validate the therapeutic potential of these EVs *in vivo* and in clinical settings. Collectively, the results of this study provide a robust scientific basis for the development of precise regenerative therapies using stem cell-derived EVs.

Acknowledgements

Not applicable.

Funding

The present study was supported by the National Research Foundation of Korea grant funded by the Korea government (grant no. RS-2024-00341119).

Availability of data and materials

The data generated in the present study may be requested from the corresponding author.

Authors' contributions

WJB obtained and analyzed the data and prepared the graphical outputs. SKK contributed to the conception and experimental design and critically revised the manuscript for important intellectual content. HSK provided expert consultation on the design of extracellular vesicle-related experiments and contributed to data interpretation. SWK contributed to data analysis and interpretation and critically revised the manuscript. JYB conceived and supervised the study, contributed to experimental design and data interpretation, critically revised the manuscript, and finalized the manuscript. SWK and JYB confirm the authenticity of all the raw data. All authors have read and approved the final version of the manuscript.

Ethics approval and consent to participate

The present study was conducted in accordance with The Declaration of Helsinki and the research design was officially approved by the Institutional Review Board of Kyung Hee University (IRB No. KHSIRB-25-417; Seoul, South Korea).

Patient consent for publication

Not applicable.

Competing interests

The authors declare that they have no competing interests.

References

1. Ray RR: Periodontitis: An oral disease with severe consequences. Appl Biochem Biotechnol 195: 17-32, 2023.
2. Sedghi LM, Bacino M and Kapila YL: Periodontal disease: The good, the bad, and the unknown. Front Cell Infect Microbiol 11: 766944, 2021.
3. Peres MA, Macpherson LMD, Weyant RJ, Daly B, Venturelli R, Mathur MR, Listl S, Celeste RK, Guarnizo-Herreño CC, Kearns C, *et al*: Oral diseases: A global public health challenge. Lancet 394: 249-260, 2019.
4. Socransky SS, Haffajee AD, Cugini MA, Smith C and Kent RL Jr: Microbial complexes in subgingival plaque. J Clin Periodontol 25: 134-144, 1998.
5. Kwon T, Lamster IB and Levin L: Current concepts in the management of periodontitis. Int Dent J 71: 462-476, 2021.
6. Lekic P and McCulloch CA: Periodontal ligament cell population: The central role of fibroblasts in creating a unique tissue. Anat Rec 245: 327-341, 1996.
7. Proff P, Reicheneder C, Faltermeier A, Kubein-Meesenburg D and Römer P: Effects of mechanical and bacterial stressors on cytokine and growth-factor expression in periodontal ligament cells. J Orofac Orthop 75: 191-202, 2014.
8. Maldonado RF, Sá-Correia I and Valvano MA: Lipopolysaccharide modification in Gram-negative bacteria during chronic infection. FEMS Microbiol Rev 40: 480-493, 2016.
9. Meng D, Wang Y and Liu T: Protective effects of silibinin on LPS-induced inflammation in human periodontal ligament cells. Front Chem 10: 1019663, 2022.
10. Yanuar A, Agustina H, Budhiparama NC and Atik N: Prospect of exosome in ligament healing: A systematical review. Stem Cells Cloning 16: 91-101, 2023.
11. Qiao X, Tang J, Dou L, Yang S, Sun Y, Mao H and Yang D: Dental pulp stem cell-derived exosomes regulate anti-inflammatory and osteogenesis in periodontal ligament stem cells and promote the repair of experimental periodontitis in rats. Int J Nanomedicine 18: 4683-4703, 2023.
12. Tao Y, Liu T, Jing F, Tan X, Zhao X, Bernaerts KV, Jia R, Zhao J, Yin Y and Zhang T: Adipose-derived stem-cell-derived exosomes encapsulated patch for modulating inflammation and promoting tissue regeneration. ACS Nano 19: 21271-21289, 2025.
13. Cho KA, Cha JE, Kim J, Kim YH, Ryu KH and Woo SY: Mesenchymal stem cell-derived exosomes attenuate TLR7-mediated mast cell activation. Tissue Eng Regen Med 19: 117-129, 2022.
14. Bae WJ, Auh QS, Kim GT, Moon JH and Kim EC: Effects of sodium tri- and hexameta-phosphate in vitro osteoblastic differentiation in Periodontal Ligament and osteoblasts, and in vivo bone regeneration. Differentiation 92: 257-269, 2016.
15. Wang J, Moosavizadeh S, Jammes M, Tabasi A, Bach T, Ryan AE and Ritter T: In-vitro immunomodulatory efficacy of extracellular vesicles derived from TGF-β1/IFN-γ dual licensed human bone marrow mesenchymal stromal cells. Stem Cell Res Ther 16: 357, 2025.
16. Livak KJ and Schmittgen TD: Analysis of relative gene expression data using real-time quantitative PCR and the 2(-Delta Delta C(T)) method. Methods 25: 402-408, 2001.
17. Zhu S, Chen W, Masson A and Li YP: Cell signaling and transcriptional regulation of osteoblast lineage commitment, differentiation, bone formation, and homeostasis. Cell Discov 10: 71, 2024.
18. Huang W, Yang S, Shao J and Li YP: Signaling and transcriptional regulation in osteoblast commitment and differentiation. Front Biosci 12: 3068-3092, 2007.

19. van Bezooijen RL, ten Dijke P, Papapoulos SE and Löwik CW: SOST/sclerostin, an osteocyte-derived negative regulator of bone formation. Cytokine Growth Factor Rev 16: 319-327, 2005.
20. Li Z, Scott MJ, Fan EK, Li Y, Liu J, Xiao G, Li S, Billiar TR, Wilson MA, Jiang Y and Fan J: Tissue damage negatively regulates LPS-induced macrophage necroptosis. Cell Death Differ 23: 1428-1447, 2016.
21. Bosco MC, Gusella GL, Espinoza-Delgado I, Longo DL and Varesio L: Interferon-gamma upregulates interleukin-8 gene expression in human monocytic cells by a posttranscriptional mechanism. Blood 83: 537-542, 1994.
22. Rodrigues DR, Fernandes RK, Balderramas HDA, Penitenti M, Bachiega TF, Calvi SA, Dias-Melicio LA, Ikoma MR and Soares ÂM: Interferon-gamma production by human neutrophils upon stimulation by IL-12, IL-15 and IL-18 and challenge with Paracoccidioides brasiliensis. Cytokine 69: 102-109, 2014.
23. Hirano T: IL-6 in inflammation, autoimmunity and cancer. Int Immunol 33: 127-148, 2021.
24. Yan L, Wang J, Cai X, Liou YC, Shen HM, Hao J, Huang C, Luo G and He W: Macrophage plasticity: Signaling pathways, tissue repair, and regeneration. MedComm (2020) 5: e658, 2024.
25. Choi DW, Cho KA, Kim J, Kim J, Lee HJ, Kim YH, Park JW and Woo SY: Extracellular vesicles from tonsil-derived mesenchymal stromal cells show anti-tumor effect via miR-199a-3p. Int J Mol Med 48: 221, 2021.
26. Ahmad P, Estrin N, Farshidfar N, Zhang Y and Miron RJ: Mechanistic insights into periodontal ligament stem cell-derived exosomes in tissue regeneration. Clin Oral Investig 29: 357, 2025.
27. Feng H, Gong S, Liu J, Aghayants S, Liu Y, Wu M, Wu Y and Song J: Adipose-derived stem cell exosomes: Mechanisms and therapeutic potentials in wound healing. Biomark Res 13: 88, 2025.
28. Tan F, Li X, Wang Z, Li J, Shahzad K and Zheng J: Clinical applications of stem cell-derived exosomes. Signal Transduct Target Ther 9: 17, 2024.
29. Ning X, Liu R, Huang Y, Huang Z, Li H, Li Q, Sheng Z and Wu J: Dental stem cell-derived exosomes: A review of their isolation, classification, functions, and mechanisms. Stem Cells Int 2024: 2187392, 2024.
30. Kim DK, Lee HJ, Lee IH and Lee JJ: Immunomodulatory effects of primed tonsil-derived mesenchymal stem cells on atopic dermatitis via B cell regulation. Cells 13: 80, 2023.
31. Shin SC, Seo Y, Park HY, Jung DW, Shin TH, Son H, Kim YK, Lee JC, Sung ES, Jang JY, *et al*: Regenerative potential of tonsil mesenchymal stem cells on surgical cutaneous defect. Cell Death Dis 9: 183, 2018.
32. Palakurthi SS, Shah B, Kapre S, Charbe N, Immanuel S, Pasham S, Thalla M, Jain A and Palakurthi S: A comprehensive review of challenges and advances in exosome-based drug delivery systems. Nanoscale Adv: Oct 29, 2024 (Epub ahead of print). doi: 10.1039/d4na00501e.

Copyright © 2026 Bae et al. This work is licensed under a Creative Commons Attribution-NonCommercial-NoDerivatives 4.0 International (CC BY-NC-ND 4.0) License.